Stabilization of a suspension of sedimenting rods by induced-charge electrophoresis

David Saintillan[a)]
Department of Mechanical Engineering, Stanford University, Stanford, California 94305

Eric S. G. Shaqfeh
Department of Chemical Engineering, Department of Mechanical Engineering, and Institute for Computational and Mathematical Engineering, Stanford University, Stanford, California 94305

Eric Darve
Department of Mechanical Engineering and Institute for Computational and Mathematical Engineering, Stanford University, Stanford, California 94305

(Received 2 October 2006; accepted 9 November 2006; published online 14 December 2006)

We use numerical simulations to investigate the dynamics in suspensions of ideally polarizable rods sedimenting under gravity in a vertical electric field. While such suspensions are unstable to concentration fluctuations when no field is applied, we show that the induced-charge electrophoresis that results from the application of the field provides control over the concentration instability by causing particle alignment in the field direction. A phase diagram is obtained for the occurrence of the instability in terms of field strength and volume fraction. In stable suspensions velocity hindrance is shown to occur, and results for the hindered settling function are presented.
 [DOI: 10.1063/1.2404948]

Controlling particle motions in fluid suspensions is of practical relevance in microfluidic applications involving colloidal dispersions. Such control can often be achieved using electric fields, which can cause the motion of charged particles in an electrolyte by electrophoresis.[1] More precisely, a particle with a fixed surface charge attracts counterions, which accumulate around the surface forming a screening cloud or electrical double layer (EDL). When an external field is applied, the migration of the excess counterions inside the EDL results in an effective slip at the surface, which can drive the motion of a freely suspended particle.[1,2]

Recent investigations have shown that uncharged polarizable objects such as metallic colloids can also be subject to an additional electrokinetic phenomenon termed induced-charge electrophoresis[3–5] (ICEP). In that case, the polarization of a particle in an electric field leads to the formation of a nonuniform charge distribution at the particle surface, which attracts a nonuniform screening cloud. As the surface charge itself is induced by the applied field, the resulting electrokinetic flow scales quadratically with field strength, and ICEP can therefore drive steady flows or motions in alternating fields. While ICEP causes no net motion for an isolated spherical particle, it can lead to the rotation of anisotropic objects such as rod-like particles,[5–8] as well as the translation of more complex asymmetric objects.[5,6] In addition, ICEP also causes relative motions in suspensions of hydrodynamically interacting particles.[7,9]

Motivated by applications using non-neutrally buoyant metallic rod-like colloids as information carriers,[10] we investigate in this Letter the dynamics in suspensions of ideally polarizable slender rods sedimenting under gravity while undergoing ICEP. The dynamics of sedimenting non-Brownian rods have been studied extensively in the past and are known to be characterized by a concentration instability.[11] This instability, which causes the particles in an initially random suspension to arrange into dense clusters with enhanced velocities,[12,13] results from the coupling between the translational and rotational motions of the particles: more precisely, the disturbance flow induced by weak density fluctuations in the suspension will cause the rods to orient in such a way that their lateral motion reinforces the fluctuations. When an electric field is applied, rotations will also occur as a result of ICEP and lead to particle alignment in the field direction:[7] this alignment will likely affect the instability by preventing the rods from rotating in the disturbance flow, and in strong fields a stabilization of the suspension may be expected.

To analyze this effect, we perform numerical simulations in periodic suspensions of uncharged polarizable interacting rods undergoing both sedimentation and ICEP, when the applied field $\boldsymbol{E}_\infty$ points in the vertical direction. The simulation method, which is presented in more detail elsewhere,[7,14] is only outlined here. We consider a collection of N slender rods of length $2l$ and aspect ratio γ, where the configuration of a given rod $\alpha=1,\ldots,N$ is determined by the position $\boldsymbol{x}_\alpha$ of its center of mass and by a unit vector $\boldsymbol{p}_\alpha$ aligned with its major axis. We also denote by s_α a linear coordinate along the rod axis. Under the assumption of thin double layers, we showed in our previous work[7] that the motion of a given rod can be modeled using slender-body theory,[15,16] which relates the linear and angular velocities of the rod to a line distribution of point force singularities $\boldsymbol{f}_\alpha(s_\alpha)$ along the rod axis,

[a)]Present address: Courant Institute of Mathematical Sciences, New York University, New York, New York 10012.

$$\dot{\boldsymbol{x}}_\alpha + s_\alpha \dot{\boldsymbol{p}}_\alpha + \tilde{\boldsymbol{u}}_s - \boldsymbol{u} = \frac{\log 2\gamma}{4\pi\mu}(\mathbf{I} + \boldsymbol{p}_\alpha \boldsymbol{p}_\alpha)\cdot \boldsymbol{f}_\alpha. \tag{1}$$

Equation (1) is the leading-order term in an asymptotic approximation valid for high-aspect ratio particles ($\gamma \gg 1$). The three variables $\tilde{\boldsymbol{u}}_s(s_\alpha)$, $\boldsymbol{u}(s_\alpha)$, and $\boldsymbol{f}_\alpha(s_\alpha)$, which denote, respectively, the circumferential average of the slip velocity induced by ICEP along the rod,[16] the disturbance fluid velocity induced by the motion of the other rods, and the force distribution along the rod of interest, must be obtained in order to determine the particle velocities. The ICEP slip velocity $\tilde{\boldsymbol{u}}_s(s_\alpha)$ was previously shown to be[7]

$$\tilde{\boldsymbol{u}}_s(s_\alpha) \approx \frac{\varepsilon}{\mu} s_\alpha (\boldsymbol{p}\cdot\tilde{\boldsymbol{E}}_\infty)\tilde{\boldsymbol{E}}_\infty + O(\gamma^{-2}), \tag{2}$$

where $\tilde{\boldsymbol{E}}_\infty$ is defined as $\tilde{\boldsymbol{E}}_\infty = \boldsymbol{\Pi}\cdot\boldsymbol{E}_\infty$ and $\boldsymbol{\Pi} = \Pi_\parallel \boldsymbol{p}_\alpha\boldsymbol{p}_\alpha + \Pi_\perp (\mathbf{I} - \boldsymbol{p}_\alpha\boldsymbol{p}_\alpha)$ is a polarizability tensor whose coefficients can be found elsewhere.[7,17] In the limit of high aspect ratio, $\boldsymbol{\Pi} \approx \mathbf{I}$. The disturbance velocity $\boldsymbol{u}(s_\alpha)$ is the fluid velocity induced by the force distributions along the rods. On rod α,

$$\boldsymbol{u}(s_\alpha) = \frac{1}{8\pi\mu}\sum_{\beta=1}^{N}\int_{-l}^{l} \mathbf{G}_p(s_\alpha - s_\beta)\cdot\boldsymbol{f}_\beta(s_\beta)\mathrm{d}s_\beta, \tag{3}$$

where $\mathbf{G}_p$ is the periodic Green's function for Stokes flow,[18] from which the Oseen tensor is subtracted when $\beta = \alpha$. Finally, the force distribution $\boldsymbol{f}_\alpha(s_\alpha)$ is obtained as a truncated Legendre polynomial expansion,[7,14]

$$\boldsymbol{f}_\alpha(s_\alpha) = \frac{\boldsymbol{F}_\alpha^{(0)}}{2l} + \frac{3s_\alpha}{2l^3}[\mathcal{S}_\alpha \boldsymbol{p}_\alpha + (\mathbf{I} - \boldsymbol{p}_\alpha\boldsymbol{p}_\alpha)\cdot\boldsymbol{F}_\alpha^{(1)}], \tag{4}$$

where $\boldsymbol{F}_\alpha^{(0)}$ and $\boldsymbol{F}_\alpha^{(1)}$ denote the zeroth and first moments of $\boldsymbol{f}_\alpha$ and are related to the total external force and torque on the rod. In particular, gravity exerts a force on each rod: $\boldsymbol{F}_\alpha^{(0),g} = -\Delta\rho V_p g\hat{\boldsymbol{z}}$, where $\Delta\rho$ is the relative density between the solid and fluid phases, V_p is the volume of a rod, and g is the acceleration of gravity. In Eq. (4), $\mathcal{S}_\alpha$ is the particle stresslet induced by the slip and disturbance velocities, and can be found as[7]

$$\mathcal{S}_\alpha = -\frac{2\pi\mu}{\log 2\gamma}\int_{-l}^{l} s\boldsymbol{p}_\alpha\cdot[\boldsymbol{u}(s_\alpha) - \tilde{\boldsymbol{u}}_s(s_\alpha)]\mathrm{d}s_\alpha. \tag{5}$$

If the zeroth and first force moments are known, Eqs. (2)–(5) can be used to write a linear system for the stresslets on all the rods. After inverting this system, the force distributions and disturbance velocities can be determined, and the rod velocities are then obtained by integration of Eq. (1),

$$\dot{\boldsymbol{x}}_\alpha = \frac{1}{2l}\int_{-l}^{l}\boldsymbol{u}(s_\alpha)\mathrm{d}s_\alpha + \frac{\log 2\gamma}{8\pi\mu l}(\mathbf{I} + \boldsymbol{p}_\alpha\boldsymbol{p}_\alpha)\cdot\boldsymbol{F}_\alpha^{(0)}, \tag{6}$$

$$\dot{\boldsymbol{p}}_\alpha = \frac{3}{2l^3}(\mathbf{I} - \boldsymbol{p}_\alpha\boldsymbol{p}_\alpha)\cdot\int_{-l}^{l} s_\alpha[\boldsymbol{u}(s_\alpha) - \tilde{\boldsymbol{u}}_s(s_\alpha)]\mathrm{d}s_\alpha + \frac{3\log 2\gamma}{8\pi\mu l^3}(\mathbf{I} - \boldsymbol{p}_\alpha\boldsymbol{p}_\alpha)\cdot\boldsymbol{F}_\alpha^{(1)}. \tag{7}$$

In addition to the gravity force $\boldsymbol{F}_\alpha^{(0),g}$, we also account for lubrication and contact forces between neighboring rods.[7,14] Equations (6) and (7) are then integrated in time to determine the particle motions.

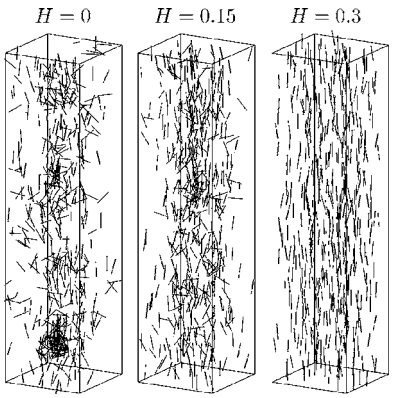

FIG. 1. Particle distributions in suspensions of 512 rods of aspect ratio $\gamma = 20$ at an effective volume fraction of $nl^3 = 0.1$ at three different field strengths: $H = 0$ (no field), 0.15, and 0.3.

In the following, we nondimensionalize the variables by the total rod length $2l$ and by the Stokes velocity $U_0 = \Delta\rho V_p g \log 2\gamma/4\pi\mu l$, or settling velocity of an isolated vertically oriented rod. The corresponding time scale $\tau_s = 8\pi\mu l^2/\Delta\rho V_p g \log 2\gamma$, or Stokes time, is the time for an isolated rod to sediment over its length. In addition to the aspect ratio γ and effective volume fraction nl^3 (where n is the mean number density), nondimensionalization of the governing equations yields the following dimensionless group H comparing the relative effects of ICEP and of gravity:

$$H = \frac{8\pi\varepsilon E_\infty^2 l^2}{\Delta\rho V_p g \log 2\gamma}. \tag{8}$$

In particular, H can be viewed as the ratio of the Stokes time τ_s to the electroviscous time $\tau_e = (\varepsilon E_\infty^2/\mu)^{-1}$, or time for fluid to convect over a rod length under the induced slip.

Typical particle distributions in suspensions of 512 rods are shown in Fig. 1 at various field strengths H. When no electric field is applied ($H = 0$), the concentration instability described above takes place and results in the formation of dense clusters falling at enhanced velocities, in good agreement with previous simulations.[14] When a weak field is applied ($H = 0.15$), the alignment of the rods in the field direction becomes visible and the instability is weaker, with the formation of fewer and less dense clusters. When a stronger field is applied ($H = 0.3$), the instability altogether disappears, and the suspension remains homogeneous. As seen in Figs. 1 and 2(b), the alignment of the rods is almost perfect, with small departures resulting from hydrodynamic interactions. As expected, ICEP therefore has a stabilizing effect on the concentration fluctuations, which results from the alignment of the rods under the applied field. Such an effect could perhaps have been expected based on our previous theory,[19] which predicts a stabilization in very anisotropic suspensions.

These observations are made more quantitative in Fig. 2, showing the time evolution of the mean settling velocity

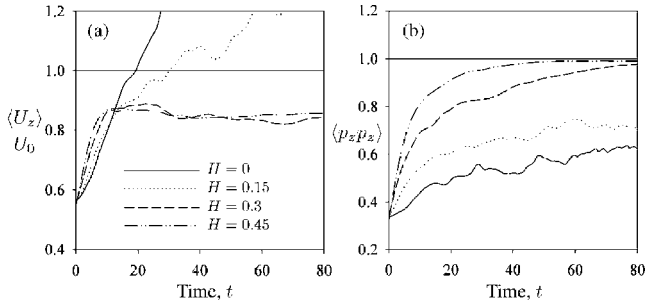

FIG. 2. Evolution of (a) the mean velocity $\langle U_z\rangle/U_0$ and (b) the orientation moment $\langle p_z p_z\rangle$ as a function of time in an initially random suspension at various electric-field strengths H, when both gravity and the electric field are applied at $t=0$.

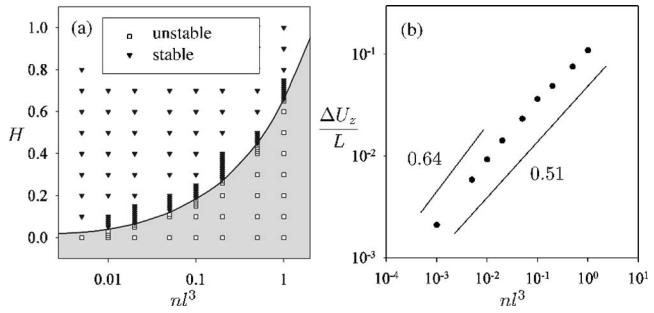

FIG. 3. (a) Phase diagram for the stability of a suspension of 512 rods of aspect ratio $\gamma=20$ sedimenting under gravity and undergoing ICEP. The criterion for stability is the existence of a steady-state settling rate below the Stokes velocity U_0. The transition between the stable and unstable regimes occurs when $H/(nl^3)^{0.54}\approx 0.65$. (b) Scaling of the vertical shear rate with the effective volume fraction nl^3, estimated as the ratio of the vertical velocity fluctuations ΔU_z to the box width L and calculated in a random isotropic suspension with no electric field ($H=0$).

$\langle U_z\rangle/U_0$ and of the second orientation moment in the vertical direction $\langle p_z p_z\rangle$. In particular, Fig. 2(a) shows that for $H=0$ and 0.15 the mean velocity increases sharply beyond the Stokes velocity, which is a direct consequence of the cluster formation resulting from the concentration instability. In stronger fields ($H=0.3$ and 0.45), the mean velocity also increases but quickly reaches a steady state below the Stokes velocity: in that case the increase is due to the alignment of the rods, while the plateau with $\langle U_z\rangle/U_0<1$ is indicative of velocity hindrance.

The effect of the electric field on the orientation is shown in Fig. 2(b). In the unstable case ($H=0$ and $H=0.15$), $\langle p_z p_z\rangle$ slowly increases as a result of the instability, which is known to cause alignment in the gravity direction:[12,14] yet the alignment is rather weak since the rods are subjected to strong fluctuations in the disturbance flow. In the stable cases, however ($H=0.3$ and 0.45), $\langle p_z p_z\rangle$ quickly reaches a plateau slightly below 1 corresponding to a very strong alignment in the suspension, which suggests that orientations are predominantly controlled by the electric field.

By repeating simulations at various field strengths and volume fractions, a phase diagram for the stabilizing effect of ICEP as a function of H and nl^3 was obtained and is shown in Fig. 3(a). The criterion used for stability is the existence of a steady-state settling velocity below the Stokes velocity. Figure 3(a) confirms that at a given volume fraction increasing the field strength causes the stabilization of the suspension beyond a certain value of H. This critical value is larger at higher volume fractions, as the velocity fluctuations that act against the alignment of the rods and cause the concentration instability are stronger in more concentrated suspensions.

The marginal stability curve in Fig. 3(a) is well captured by the following power law: $H/(nl^3)^{0.54}\approx 0.65$, which can be rationalized by a simple argument. If the stabilizing effect of ICEP is a consequence of particle alignment, the onset of instability should occur when the angular velocities resulting from ICEP and from the velocity fluctuations induced by sedimentation are balanced,

$$|\dot{\boldsymbol{p}}_{\mathrm{ICEP}}|/|\dot{\boldsymbol{p}}_{\mathrm{SED}}|\approx O(1). \tag{9}$$

From Eqs. (2) and (7) one can show that the ICEP angular velocity scales as the inverse of the electroviscous time: $|\dot{\boldsymbol{p}}_{\mathrm{ICEP}}|\sim\varepsilon E_\infty^2/\mu$. On the other hand, the angular velocity induced by sedimentation must scale with the effective shear rate of the disturbance flow induced by the settling of the suspension $|\dot{\boldsymbol{p}}_{\mathrm{SED}}|\sim\dot{\gamma}_{\mathrm{SED}}$. The disturbance flow is driven by the density fluctuations in the particle distribution, and in a random suspension, occurs on length scales comparable to the width of the container. Its shear rate can be estimated by the ratio $\langle\Delta U_z\rangle/L$ of the particle velocity fluctuations to the container size, which is plotted in Fig. 3(b). In particular, the following scaling is found: $\dot{\gamma}_{\mathrm{SED}}\sim(U_0/l)(nl^3)^{0.51}$, from which the stability criterion, Eq. (9), becomes $H/(nl^3)^{0.51}\approx O(1)$, in good agreement with the scaling found in Fig. 3(a).

At very low volume fractions, a slightly higher exponent of 0.64 is predicted by Fig. 3(b). This value can be explained by balancing the buoyancy and viscous forces acting on the long-wavelength Poisson density fluctuations in a dilute random suspension,[20] resulting in a shear rate $\dot{\gamma}_{\mathrm{SED}}\sim(U_0/l)\times(nl^3)^{1/2}(L/l)^{-1/2}$. In the simulations of Fig. 3, the box size was chosen to maintain a constant number of particles, in which case $L\sim(nl^3)^{-1/3}$. The scaling for the shear rate then becomes $\dot{\gamma}_{\mathrm{SED}}\sim(U_0/l)(nl^3)^{2/3}$, hence an expected exponent of 2/3. The departure from this ideal value at higher concentrations may be a result of the small system sizes and of nonlocal interactions between the rods, and goes beyond the scope of this Letter. One should also note that the scaling for $|\dot{\boldsymbol{p}}_{\mathrm{SED}}|$ depends on the suspension microstructure: in a nonrandom suspension a different scaling may occur, and may modify the stability diagram of Fig. 3(a). However, we expect the general criterion of Eq. (9) to remain valid in general.

Results for the settling velocity in stable suspensions are shown in Fig. 4. Note that the mean velocity only results from sedimentation, as ICEP does not create a net motion for particles with fore-aft symmetry.[5–7] As previously observed in Fig. 2(a), the steady-state velocity is less than the Stokes velocity, and slowly increases with H as a result of the stronger alignment of the rods [Fig. 4(a)]. At high values of H, the velocity reaches a plateau: this suggests that the dominant

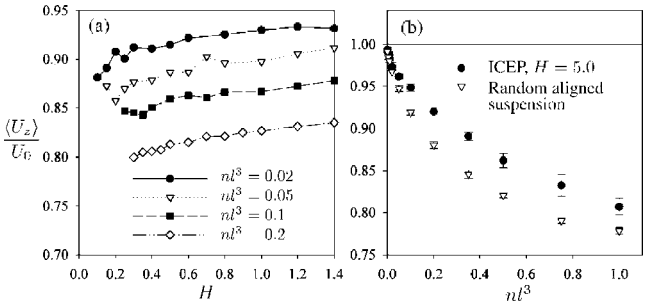

FIG. 4. Steady-state settling rate $\langle U_z \rangle / U_0$ in suspensions of 512 rods of aspect ratio $\gamma=20$ as a function of (a) the field strength H at various volume fractions, and (b) the effective volume fraction nl^3 at a field strength of $H=5.0$. Plot (b) also shows the settling rate in a random suspension of aligned rods.

effect of ICEP is to control the particle orientations and suspension microstructure.

The hindered settling function $\langle U_z \rangle / U_0$ versus nl^3 is shown in Fig. 4(b) in a strong field ($H=5.0$), at which the suspension alignment is very strong: $\langle p_z p_z \rangle \geq 0.99$. Beyond such a value of H the effect of increasing field strength becomes negligible. Figure 4(b) also shows the settling rate in a random suspension of perfectly aligned rods. As expected, the hindered settling function, which is 1 in the limit of infinite dilution, decreases with effective volume fraction nl^3. Note that the dependence of $\langle U_z \rangle / U_0$ on nl^3 is nonlinear even at the lowest volume fractions: this is a consequence of the periodic boundary conditions used in the simulations,[18,21] and would not be observed in a nonperiodic suspension. Interestingly, we find that the settling rate in the stable suspension undergoing ICEP slightly exceeds that in the random suspension of aligned rods. This small discrepancy suggests that a nonuniform microstructure still exists in stable suspensions undergoing ICEP: as shown in our previous work,[7] ICEP indeed results in particle pairings which are likely to be responsible for the observed velocity enhancement.

In summary, we have demonstrated that the application of an electric field in a suspension of polarizable rods settling under gravity can be used to control or suppress the concentration instability that otherwise occurs in these systems. A simple scaling argument was used to predict the transition between unstable and stable regimes, based on a balance between ICEP and flow-induced rotations. In stable suspensions, velocity hindrance was observed to occur as a result of hydrodynamic interactions, and the hindered settling function was shown to slightly exceed that of a random suspension of aligned rods. While the present study presented one method for suppressing the concentration instability in suspensions of sedimenting rods, it also suggests that other means of controlling particle orientations (for instance, using imposed flows) may result in stabilization as well.

D.S. gratefully acknowledges funding from a Gerald J. Lieberman Graduate Fellowship.

[1] D. A. Saville, "Electrokinetic effects with small particles," Annu. Rev. Fluid Mech. **9**, 321 (1977).
[2] W. B. Russel, D. A. Saville, and W. R. Schowalter, *Colloidal Dispersions* (Cambridge University Press, Cambridge, 1989).
[3] M. Z. Bazant and T. M. Squires, "Induced-charge electrokinetic phenomena: theory and microfluidic applications," Phys. Rev. Lett. **92**, 066101 (2004).
[4] T. M. Squires and M. Z. Bazant, "Induced-charge electro-osmosis," J. Fluid Mech. **509**, 217 (2004).
[5] T. M. Squires and M. Z. Bazant, "Breaking symmetries in induced-charge electro-osmosis and electrophoresis," J. Fluid Mech. **560**, 65 (2006).
[6] E. Yariv, "Induced-charge electrophoresis of nonspherical particles," Phys. Fluids **17**, 051702 (2005).
[7] D. Saintillan, E. Darve, and E. S. G. Shaqfeh, "Hydrodynamic interactions in the induced-charge electrophoresis of colloidal rod dispersions," J. Fluid Mech. **563**, 223 (2006).
[8] K. A. Rose, J. A. Meier, G. M. Dougherty, and J. G. Santiago, "Rotational electrophoresis of striped metallic microrods," Phys. Rev. E (in press).
[9] A. S. Dukhin and V. A. Murtsovkin, "Pair interaction of particles in electric field. 2. Influence of polarization of double layer of dielectric particles on their hydrodynamic interaction in a stationary electric field," Colloid J. USSR **48**, 203 (1986).
[10] S. R. Nicerwarner-Peña, R. G. Freeman, B. D. Reiss, L. He, D. J. Peña, I. D. Walton, R. Cromer, C. D. Keating, and M. J. Natan, "Submicrometer metallic barcodes," Science **294**, 137 (2001).
[11] D. L. Koch and E. S. G. Shaqfeh, "The instability of a dispersion of sedimenting spheroids," J. Fluid Mech. **209**, 521 (1989).
[12] D. Saintillan, E. S. G. Shaqfeh, and E. Darve, "The growth of concentration fluctuations in dilute dispersions of orientable and deformable particles under sedimentation," J. Fluid Mech. **553**, 347 (2006).
[13] B. Metzger, É. Guazzelli, and J. E. Butler, "Large-scale streamers in the sedimentation of a dilute fiber suspension," Phys. Rev. Lett. **95**, 164506 (2005).
[14] D. Saintillan, E. Darve, and E. S. G. Shaqfeh, "A smooth particle-mesh Ewald algorithm for Stokes suspension simulations: The sedimentation of fibers," Phys. Fluids **17**, 033301 (2005).
[15] G. K. Batchelor, "Slender-body theory for particles of arbitrary cross-section in Stokes flow," J. Fluid Mech. **44**, 419 (1970).
[16] Y. Solomentsev and J. L. Anderson, "Electrophoresis of slender particles," J. Fluid Mech. **279**, 197 (1994).
[17] S. P. Han and S.-M. Yang, "Orientation distribution and electrophoretic motions of rod-like particles in a capillary," J. Colloid Interface Sci. **177**, 132 (1996).
[18] H. Hasimoto, "On the periodic fundamental solutions of the Stokes equations and their application to viscous flow past a cubic array of spheres," J. Fluid Mech. **5**, 317 (1959).
[19] D. Saintillan, E. S. G. Shaqfeh, and E. Darve, "The effect of stratification on the wavenumber selection in the instability of sedimenting spheroids," Phys. Fluids **18**, 121503 (2006).
[20] R. E. Caflisch and J. H. C. Luke, "Variance in the sedimentation speed of a suspension," Phys. Fluids **28**, 759 (1985).
[21] P. G. Saffman, "On the settling speed of free and fixed suspensions," Stud. Appl. Math. **52**, 115 (1973).